ADVANCED ENERGY & SUSTAINABILITY RESEARCH
Open Access
www.advenergysustres.com

Scalable Fabrication of Black Cu-Embedded Polydimethylsiloxane for Enhancing Triboelectric Nanogenerator Performance in Energy Harvesting and Self-Powered Sensing

*Mengyan Yang and Tao Hua**

Triboelectric nanogenerators (TENGs) are widely used in self-powered electronic devices and tactile sensors. Herein, for the first time, the facile, low-cost, and universal electroless deposition (ELD) technology is used to fabricate nonconductive black Cu to enhance the electrical output performance and sensitivities of TENG-based tactile sensor. The output performance and sensitivities of the equipment are significantly improved by the introduction of black Cu nanoparticles (NPs) coated cellulose filter paper (CFP) into the polydimethylsiloxane (PDMS) matrix. With an optimal load of black Cu NPs, the composite film-based TENG produces the highest surface charge density exhibited by high sensitivities of 1.56 V N^{-1}, 3.5 times of that obtained via PDMS-based TENG under the same conditions. These properties facilitate the developed device to be competent at monitoring a kind of human movements, such as finger touching and bending. The proposed strategy not only demonstrates a promising potential of developing large-scale practical self-charging equipment and improving the output performance and sensitivities of TENG based tactile sensors but also provides a new perspective for applications in other fields.

1. Introduction

Wearable electronic devices are attracting more and more attention to motion detection, tactile sensing, and biomedical signal monitoring.[1–4] However, current commercial wearable electronic devices still require external power supplies and the collaborative work of multiple devices, rather than highly versatile integration. Looking for portable power sources and developing self-charging devices are one of the most potential methods to settle the traditional bulky, nonremovable, and integrated energy supply modes.[5–8] Mechanical energy is one of the most plentiful energy sources in nature. It has a wide range of sources, is easy to obtain, and can exist independently. The real-time collection and conversion of mechanical energy are expected to achieve a kind of sustainable, inexhaustible, and self-charging multifunctional portable power source.[9–11] Triboelectric nanogenerator (TENG), which works by combining the electrostatic induction and contact electrification together, has been proved to be a promising technology for converting collected mechanical energy into electrical energy.[12–16] With a variety of operating modes, low cost, simple manufacturing process, a wide choice of materials, and high power output ability, the research enthusiasm in TENG as a mechanical energy collection device for self-charging electronic applications and sensors is growing rapidly.[17–19] As an abundant supply of mechanical energy, people can achieve self-sufficiency in TENG by obtaining energy from human movements.[20–22]

The flexible TENG is light, wearable, and highly deformable, so it is becoming a very potential candidate to satisfy the development of portable electronic devices. By adopting a combination of friction materials with a larger difference in electronegativity, modifying materials,[23] or using innovative equipment structures,[24] great efforts have been made to improve the output performance of TENG.[25,26] Nonetheless, seeking suitable friction materials is still a huge challenge for durable, wearable, and flexible high performance TENG. Polydimethylsiloxane (PDMS) as an elastic, transparent, and hydrophobic polymer with outstanding electronegativity, which imparts high water resistance and long-term stability to the TENG, has been researched and used in kinds of TENGs.[27–29] However, it is not a very efficient triboelectric material, and PDMS worked alone is not appropriate for preparing high-performance TENG. Therefore, many methods have been studied to modify PDMS for enhancing the power generation of PDMS-based TENG. In previous studies, some metal oxide materials including $BaTiO_3$,[30,31] $SrTiO_3$,[32] ZnO,[33,34] AlO_x,[35] and other conductive nanomaterials, such as Ag[36] and Au NPs,[37,38] Mxene,[39,40] and carbon materials[41–43] have been adopted as filler in polymer precursor to adjust the surface charge

M. Yang, T. Hua
Nanotechnology Center
Institute of Textiles & Clothing
The Hong Kong Polytechnic University
Hung Hom, Kowloon 999077, Hong Kong
E-mail: tcthua@polyu.edu.hk

The ORCID identification number(s) for the author(s) of this article can be found under https://doi.org/10.1002/aesr.202100116.

DOI: 10.1002/aesr.202100116

density by adjusting their work functions or dielectric constant to enhance the overall output performance of TENG. Numerous researches have proven that mixing PDMS with the aforementioned metal oxide or conductive materials are able to increase the output performance of TENG.[44] However, these materials are high cost or require complicated fabrication techniques. Therefore, it is important to find conductive fillers with simple preparation processing, low cost, and large-scale production. Unlike the above conductive fillers, black copper is low cost and can be produced on a large scale due to its simple and diverse preparation methods. The primary function of black Cu NPs is to raise the surface charge density by decreasing its internal resistance and enhancing the dielectric property of PDMS and enlarging the capacitance of the TENG, thereby improving the power output of TENG. These attractive and exclusive functions enable this improved composite film to be a promising material for obtaining high-power output devices.

On the contrary, the successful optimization of functional composites depends not only on the inherent characteristics of nanofillers but also on the interface interaction between the filler and polymer and uniform distribution of the filler inside the polymer body. However, in the traditional stirring and mixing method model,[38,43,45,46] some NPs tend to disperse on the surface of PDMS and agglomerate to a certain extent, which reduces the effective dielectric property, resulting in a decrease in the power output of TENG. It is well known that electroless deposition (ELD) is particularly attractive for fabricating metal NPs on the surface of substrates to produce flexible conductive electrodes on a large scale because it can be conducted under environmental conditions without any expensive equipment.[47] Therefore, we fabricated black Cu based on CFP substrate by simply adjusting the concentration of the metal plating solution and the plating time by understanding the metal ELD nucleation, growth, and structure. CFP is used with a large surface area to load black Cu NPs, and then embedding them in PDMS to avoid the agglomeration of black Cu NPs and the exposure to the outside of PDMS, thereby avoiding reducing the dielectric property of PDMS. At the same time, the thickness of the electronegative friction layer is reduced due to the decrease in the amount of PDMS, which further improves the power output of the device.

Herein, for the first time, we propose to use the simple, low-cost, and versatile electroless deposition (ELD) technology in a new way to fabricate nonconductive black Cu to promote the output performance and sensitivities of TENG-based sensors. It is found that the incorporation of black Cu-coated CFP in the PDMS matrix has a remarkable influence on the electrical output performance of the TENG. Meanwhile, CFP is used to load black Cu NPs to ensure them more uniformly embedded in the PDMS and avoid exposure to the outside. Moreover, a self-charging tactile sensor based on the improved TENG is demonstrated, which exhibits high sensitivity and well linear correlation. Meanwhile, due to the wide application of black metals in catalysis, photothermal conversion, and other fields, such a novel extension of ELD technology can not only improve the output performance of TENG, but also provide a new perspective for inspiring excellent applications in the fields of wearable devices, artificial skin, catalysis, photothermal conversion, biomedical industries, and so on.

2. Results and Discussion

As shown in **Figure 1**, the fabrication of black Cu-coated CFP includes TA modification,[48] catalyst immobilization, and metal ELD. In short, first, by immersing the CFP in the TA aqueous solution, the TA was attached to the surface of the CFP through intermolecular hydrogen bonds. TA is a common mordant used in the dyeing process for cellulose fibers such as cotton. The role of TA is mainly as a designed interface via dip coating and subsequent catalyst-activated ELD. This polymerized phenol-rich coating provides enough sites to anchor the catalyst for subsequent ELD. After drying, the black Cu-coated CFP film was immersed in the PDMS precursor once and then the composite film coated with the PDMS prepolymer was cured in an oven. After that, the prepared PDMS-black Cu-CFP composite was cut into a square of $2.5 \times 2.5\ cm^2$. The PDMS-black Cu-CFP composite was attached to the Al foil resulting in the TENG device.

The successful modification of TA on the surface of CFP was confirmed by Fourier transform infrared spectroscopy (FTIR). From **Figure 2**a, original and CFP with TA coating is compared, the new peak near $1715\ cm^{-1}$ is attributed to the C═O stretching of the carbonyl group in TA, and the C═C tensile vibration of the aromatic group in TA generates a medium strength band at $1605\ cm^{-1}$. After TA coating, the TA-modified CFP was immersed in a $1\ g\ L^{-1}$ $(NH_4)_2PdCl_4$ aqueous solution to fix the catalysts for 15 min. In the catalytic system, the reaction mechanism between TA and $PdCL_4^{2-}$ is very crucial and can influence the subsequent catalytic efficiency. Thus, XPS was adopted to identify the chemical composition on the surface of the $PdCl_4^{2-}$ immobilized CFP composite film. From Figure 2b, through XPS analysis, the peaks at 343.1 (Pd $3d_{3/2}$), and 337.3 eV (Pd $3d_{5/2}$) confirm that $PdCl_4^{2-}$ was successfully immobilized on the TA-modified CFP substrate during the ion exchange process. The crystalline structure of black Cu deposited on the surface of CFP was detected by X-ray diffraction (XRD). As shown in Figure 2c, The XRD spectrum of black Cu-coated CFP shows three main peaks at 2θ values of 43.2°, 50.4°, and 74.3° corresponding to the (111), (200), and (220) planes, respectively.

The morphology of the obtained black Cu NPs was observed using a SEM. Generally, CFP is made of cotton/pulp with a porous structure, and the pore structure plays a key role in preventing small black Cu NPs from connecting to form a conductive metal film. For this reason, black Cu-coated CFP, fabricated by our approach, is discussed in the SEM characterization. Figure 2 shows the SEM graphs of unmodified CFP (d), black Cu-coated CFP (e–g), and the digital photograph of black Cu-coated CFP (h). It can be obviously seen that the surface morphology of the untreated CFP and black Cu-modified CFP has significant changes. As shown in Figure 2f,g, black Cu NPs are very homogeneously dispersed on the surface of CFP. The shapes of the black Cu NPs include nanospheres and nanoclusters, and the average size of the black Cu NPs is 58 ± 15 nm, which is much smaller than the pore size of CFP with 10–15 μm (Figure S1, Supporting Information). To date, nonresonant absorption has been demonstrated by suppressing the reflection of light through a combination of using nano- and microstructured surface modification and with composite material containing metal NPs embedded in dielectric materials to turn shiny metals black.[49] Thus, we control the size of Cu

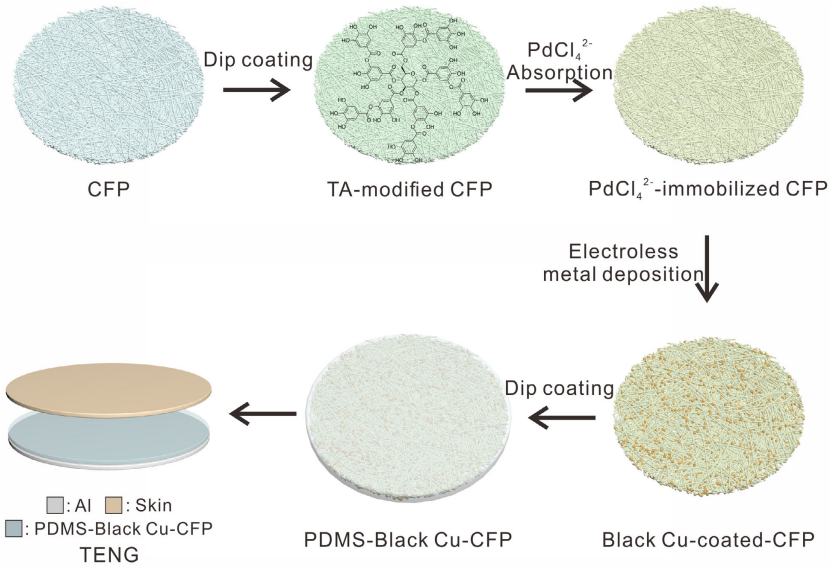

Figure 1. The schematic diagram for electroless deposition of black Cu and the fabrication of TENG.

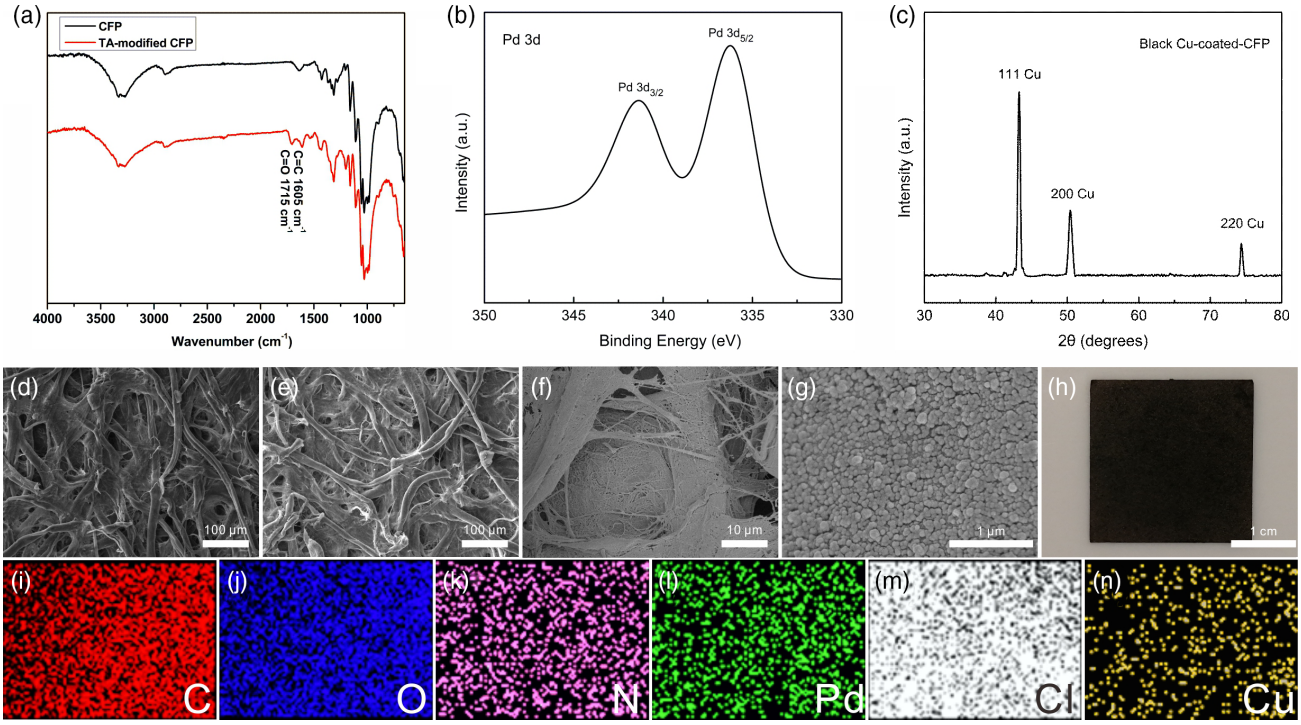

Figure 2. a) FTIR spectrum of the CFP without any treating and with TA modification. b) XPS spectra of Pd 3*d* in the $PdCl_4^{2-}$ immobilized CFP film. c) The XRD spectrum of black Cu-coated CFP. SEM photographs of CFP d) without any modification and e–g) with the black Cu coating (6 min ELD). h) Photo of black Cu-coated CFP (6 min ELD). i–n) EDS map of Cu-coated CFP (6 min ELD).

NPs by adjusting the concentration of the metal plating bath and the ELD time to obtain black Cu.

The SEM and the EDS analysis of the black Cu-coated CFP confirmed the presence of Cu NPs. In addition, as shown in Figure 2i–n, the EDS mapping images were performed to analyze the elemental distribution. The results show that C, O, N, Cl, Pd, and Cu elements are evenly distributed on the surface of CFP. The N, Cl, and Pd elements may be introduced during the ion-exchange process. From Figure 2n, it can be seen that black Cu NPs showed good dispersity without significant agglomeration on the surface of CFP.

As the mass of CFP is very light, an increase in the weight of black Cu NPs can be observed during the ELD process. As shown in **Figure 3**a, the weight of black Cu-coated CFP increases as a

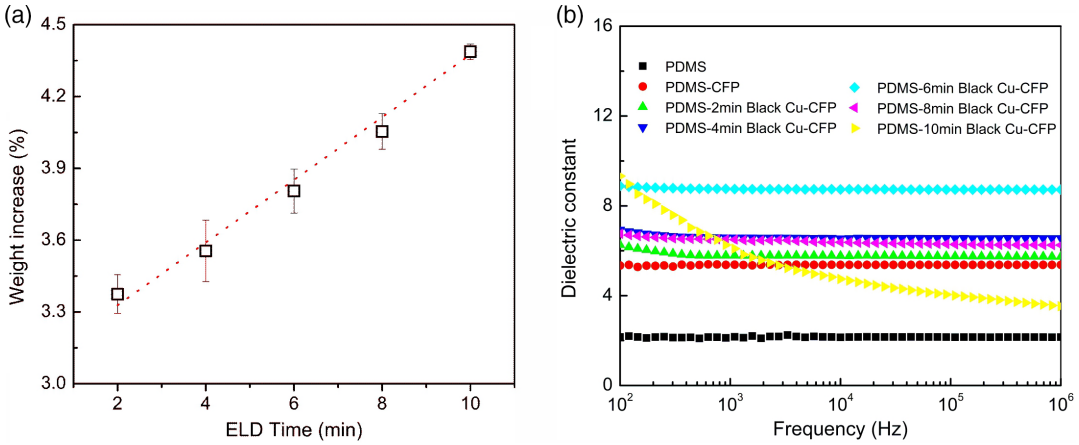

Figure 3. a) Weight increase in Cu-coated CFP change with the ELD plating times. b) Dielectric constant in the frequency range of 10^2–10^6 Hz of PDMS, PDMS-CFP, PDMS-black Cu-CFP composite films.

first-order function of ELD time, reaching about 4.38% after 10 min of metal ELD. Meanwhile, the electrical resistance of black Cu-coated CFP samples was connected with a multimeter (resistance channel) to detect. Before 8 min of ELD on Pd-modified CFP, the obtained composite films exhibit electrical insulation. But in the case of 10-min ELD, Cu-coated CFP turns into electrically conductive, and the resistance reaches approximately 0.376 MΩ cm^{-1}. This is because with the increase in ELD time, the Cu NPs are becoming more and more and likely to agglomerate and form a conductive network in the surface of CFP. At this time, the obtained Cu-coated CFP is not black but shows the color of metallic copper (Figure S2, Supporting Information). Meanwhile, we measured the dielectric properties of the composite films. Figure 3b shows the frequency-dependent dielectric constant of PDMS, PDMS-CFP, PDMS-black Cu-CFP composite films. It can be seen that with the addition of black Cu, the dielectric constant increases from 2.15 for PDMS to 5.28 for PDMS-CFP and 8.89 for PDMS-6 min black Cu-CFP, then decreases to 6.26 for PDMS-8 min black Cu-CFP. The addition of black Cu in the polymer will form a particle–polymer interface and due to the different relaxation time between NPs and PDMS, interface polarization occurs, also known as Maxwell–Wanger–Sillars polarization, resulting in accumulated charges on these interfaces.[44] This results in an increase in the dielectric constant of the composite film containing black Cu. However, when the black Cu continues to increase and lead to agglomeration, which reduces the dielectric properties of PDMS. The dielectric constant of these composite materials is almost stable within a frequency range of 10^2–10^6 Hz, except for the PDMS-black Cu-CFP composite film with the ELD time of 10 min. As the amount of PDMS is very small, the thickness of the composite films is about 231 ± 5 um. When the ELD time exceeds 10 min, the amount of PDMS is not enough, so the composite film is still in a conductive state with a resistance of 0.619 MΩ cm^{-1}. Therefore, the dielectric constant of the PDMS-10 min black Cu-CFP composite film shows a downward trend within the frequency range of 10^2–10^6 Hz.

The working mechanism of TENG is mainly based on the combination of triboelectrification and electrostatic induction.[50] As shown in **Figure 4**a–d, first, the device remains electrically neutral without any external force. Due to electrostatic induction, when the skin is separated from the PDMS-black Cu-CFP, the triboelectric charge generated on the friction layer can generate a corresponding induced charge on the Al foil electrode, thereby building the electric current in the external circuit. When the skin is far away from PDMS-black Cu-CFP composite film to a certain extent, all the triboelectric charge has been completely shielded by induced charge generated on the electrode. Therefore, no electrical signal is observed. Once the skin approaches the PDMS-black Cu-CFP composite film again, the equilibrium state may be destroyed. Thereby, electrons will flow back to generate an opposite output current. When the skin and the PDMS-black Cu-CFP composite film are tightly attached, there is no potential difference between the skin and PDMS black Cu-CFP surface because the opposite charges almost overlap on the same plane. Here, hand hammering was used as an example. As shown in Figure 4e,f, when the flexible TENG was periodically hammered by a human hand, the TENG (2.5×2.5 cm^2) produced a high output voltage of 180 V and a current of 2.9 μA.

In addition, COMSOL software was used to simulate the potential distribution of TENG through finite element analysis (FEA) in the open-circuit state. In the contact state, the opposite charges induced on the simulated skin layer (Al foil) and the PDMS-black Cu-CFP composite film neutralize each other, resulting in no potential difference between the upper and lower Al foil. Once upper Al foil is separated from its counterpart, the triboelectric charge remains on the surface of PDMS-black Cu-CFP composite material and establishes an open voltage between the two Al foils (Figure S3, Supporting Information).

We used Al foil to replace the skin as the positive friction material and to simulate the actual working situation of the self-powered sensor in close contact with the human body during real work; only double-sided tape (thickness: 80 μm) was used as an insulator between the simulated skin layer (Al foil) and the PDMS-black Cu-coated CFP film. A keyboard machine was used to quantitatively measure the electrical output performance of TENG, including open-circuit voltage, short-circuit current, and short-circuit charge transfer. From **Figure 5**a–c, we measured the open voltage, current, and charge transfer, which were produced by the pure PDMS, PDMS-CFP, and PDMS-black Cu-CFP composite film with the ELD of 6 min based TENGs,

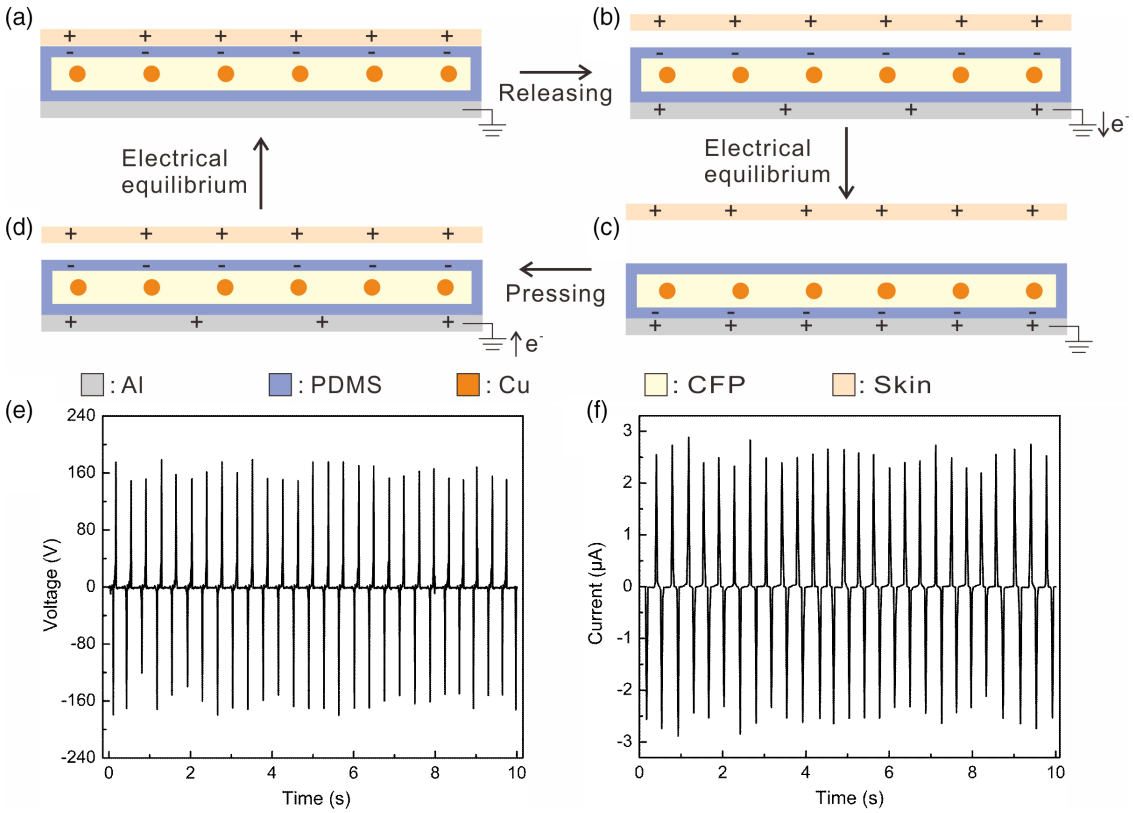

Figure 4. a–d) Schematic diagram of the working mechanism of TENG. e) Output voltage and f) current of the TENG under periodic manual hammering.

respectively, at a periodic compression force of 10 N and kept a steady frequency of 2.5 Hz. With the addition of CFP, the output voltage, current, and charge transfer increased. The output current is due to the transfer of electric charge through the external circuit during the reciprocating motion of the two friction layers. Under the same applied force, the output voltage of the TENGs based on PDMS-CFP and PDMS-black Cu-CFP with the ELD of 6 min is about 1.6 and 4 times higher than the obtained via TENG based on the pure PDMS, respectively. It is because the introduction of CFP with pore structure avoids the agglomeration of black Cu NPs and the exposure to the surface of PDMS for reducing the dielectric property of PDMS. At the same time, due to the reduction in the amount of PDMS, the thickness of the friction layer is reduced, which further boosts the output performance of the device.

The effect of different loadings of black Cu NPs under different ELD time on the TENG's electrical output performance was further investigated. During the test process, the external applied force and frequency were kept a constant at 50 N and 2.5 Hz, respectively. First of all, the weight increase and conductivity of black Cu-CFP films with different ELD time and the dielectric constant of the composite films were studied, and the corresponding data are shown in Figure 3a,b. As shown in Figure 5d–f, the output voltage, current, and charge transfer of the PDMS-black Cu-CFP-based TENG increase gradually with the rise of black Cu NPs within the ELD time range of 2–6 min, respectively, which means that an extended ELD time in this time range can significantly enhance the output performance. The addition of black Cu NP will reduce the internal resistance of pure PDMS and increase the capacitance of the wearable TENG, resulting in improved output performance. When the ELD time is 6 min, the output voltage rises to a maximum of 68 V. Unexpectedly, as the ELD time is further extended, the output performance drops slightly in the longer ELD time range. These indicate that too long ELD time cannot make a significant improvement to the increase in output voltage, and the electrical output performance is seriously influenced once the ELD time exceeds 8 min. The Cu NPs with longer ELD time increase and likely agglomerate and form a conductive network on the surface of CFP, thereby weakening the dielectric property of PDMS. Accordingly, the electricity leakage phenomenon may have a negative effect on the output performance of the device. How the dielectric properties of the PDMS film with adding black Cu affects the output performance of the TENG, a more detailed discussion is provided in Figure S4, Supporting Information. Therefore, in the following section, PDMS-black Cu-CFP with the ELD time of 6 min will be chosen to prepare TENG.

The influence of external applied forces on the electrical performance of the wearable TENG (2.5 × 2.5 cm^2) was also systematically explored. The electric output performance generated by the PDMS-black Cu-CFP-based TENG device was detected when the TENG was applied to a certain range of external force (10–50 N). As shown in **Figure 6**a, the output voltage rises as the applied force raises, and when the applied force is greater than 40 N, the output voltage increases slowly. The current and charge

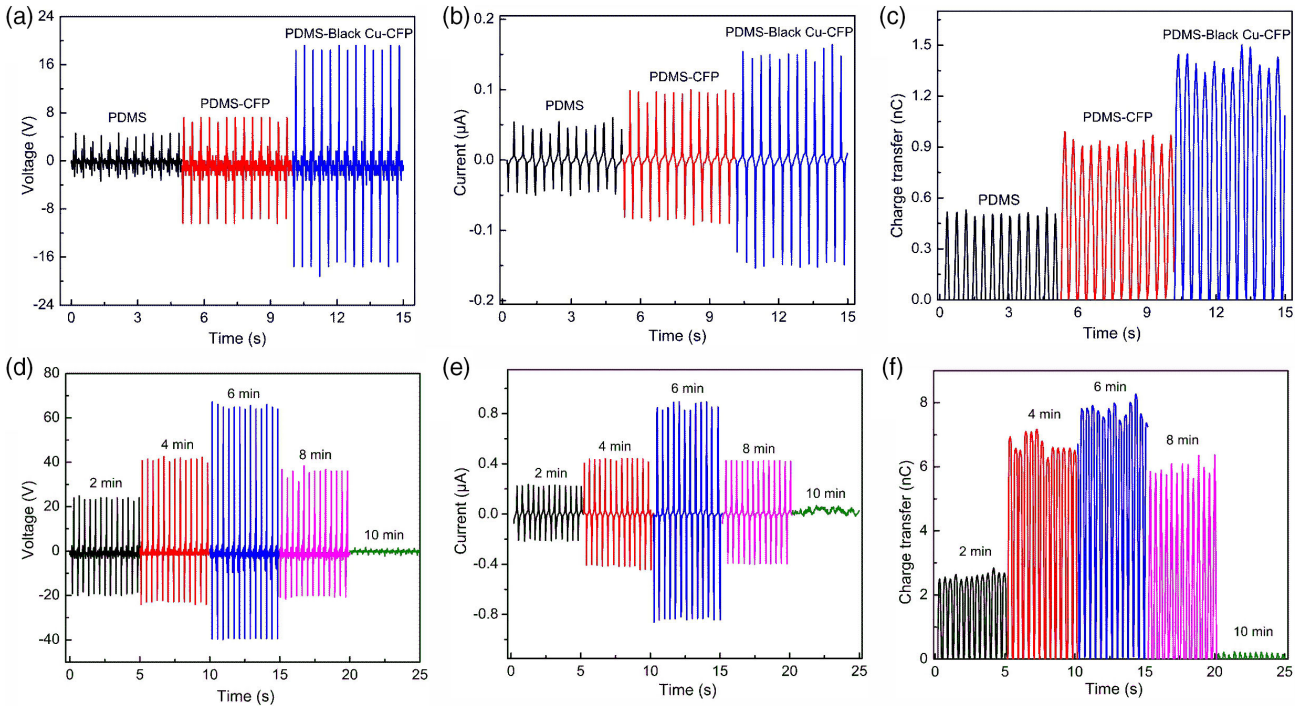

Figure 5. Electrical output performance: a) output voltage, b) current, and c) charge transfer of a PDMS, PDMS-CFP, and PDMS-black Cu-CFP-based TENG (6 min ELD). PDMS-black Cu-CFP films prepared with different ELD times, including d) output voltage, e) current, and f) charge transfer.

transfer in Figure 6b,c also exhibit the same trend. As a result, increasing the external applied force on the TENG is an efficient method to enhance its output performance.

As shown in Figure 6d, when the external force rises from 10 to 50 N, the output voltage of TENG (2.5×2.5 cm^2) rises rapidly from 19 to 68 V. Under the applied force of 10–30 N corresponding to 16–48 kPa, the output voltage rises relatively quickly from 19 to 50 V with the applied force. The high linear sensitivity of the force and pressure sensor of TENG based on PDMS-Black Cu-CFP are about 1.56 V N^{-1} and 0.98 V kPa^{-1}, respectively. Compared with a pure PDMS-based TENG, the sensitivity is increased by 3.5 times under the same mechanical force. Compared with the TENG force/pressure sensors listed in Table S1, Supporting Information, our excellent sensitivity of the sensor based on PDMS-black Cu-CFP TENG is much higher than the conventional TENGs of about 0.317–1.03 V N^{-1} and 0.06–0.29 V kPa^{-1}, respectively.

The output voltage, current, and charge transfer of TENG under different frequencies are also investigated (50 N). As shown in Figure 6e,f, as the strike frequency increases from 1 to 5 Hz, the output voltage is approximately stable; the charge transfer also exhibits the same trend. The current increases accordingly with the operation frequency (Figure S5, Supporting Information).

To exhibit the potential practical applications of the energy harvesting equipment that has been developed, commercially available capacitors and LEDs were charged and powered, respectively. The working electrical circuit of the power supply system based on flexible TENG is shown in **Figure 7**a. The bridge rectifier was connected between the flexible TENG and six different commercial capacitors (1–100 μF) to achieve the power supply (Figure 7b). At the same time, a 1 μF capacitor can be rapidly charged to 31.3 V in 60 s, which shows that the fast charging potential of TENG can be used for the subsequent power small electronic devices.

Furthermore, as shown in Figure 7c, we applied this flexible TENG (2.5×2.5 cm^2) as a power source at powering 62 commercial LEDs connected in series (Movie S1, Supporting Information). The TENG was directly driven by repeated hand hammering without any additional energy storage equipment. Our manufacturing method is easy to expand, so it is possible to produce large-scale TENG, which can generate sufficient energy to drive commercial electronic equipment. The TENG may also be used as flexible self-charging sensors including touch or pressure sensor, cardiac sensor, and pulse sensor for healthcare and security monitoring.

The electrical output under various external load resistances was systematically investigated. As shown in Figure 7d, a relationship curve between the output voltage and load resistances ranging from 10^5 to 10^9 Ω was measured by connecting various resistors to the TENG. The result shows that the output voltage is gradually increased with the rise of the external load resistor; while owing to the ohmic loss, the current curve shows the opposite trend. Meanwhile, the output power density of the TENG was further studied based on the triboelectric output performance of the device. The instantaneous output power is calculated by the following formula, $P = U^2/R$, where U and R represent the output voltage of the TENG and the load resistance, respectively.[51] As shown in Figure 7e, with the increase in load resistance, the output power density initially rises and then decreases. In terms of the maximum power transfer theorem, the maximum output power may be obtained because the resistance of the external

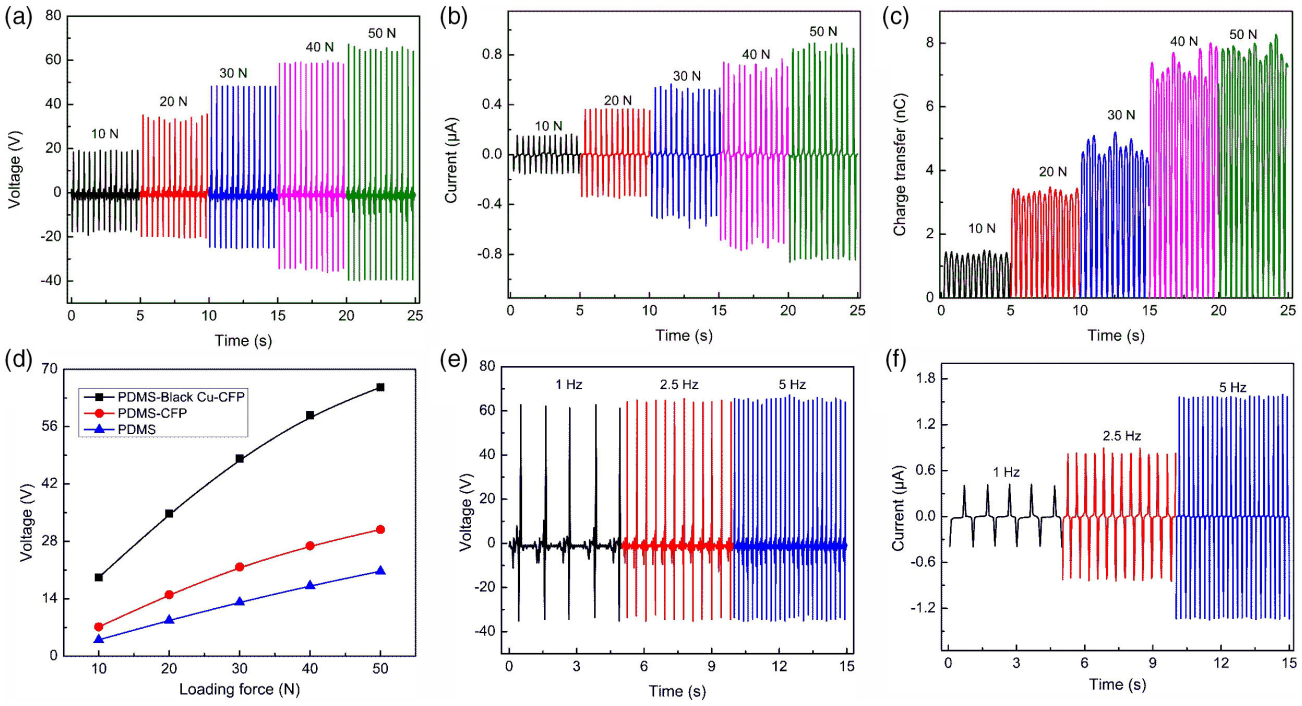

Figure 6. Electrical output performance: a) output voltage, b) current, and c) charge transfer of PDMS-black Cu-CFP based TENG d) output voltage of the sensors with different applied forces under a constant frequency of 2.5 Hz. e) Output voltage and f) current of the TENG with different loading frequencies (1–5 Hz).

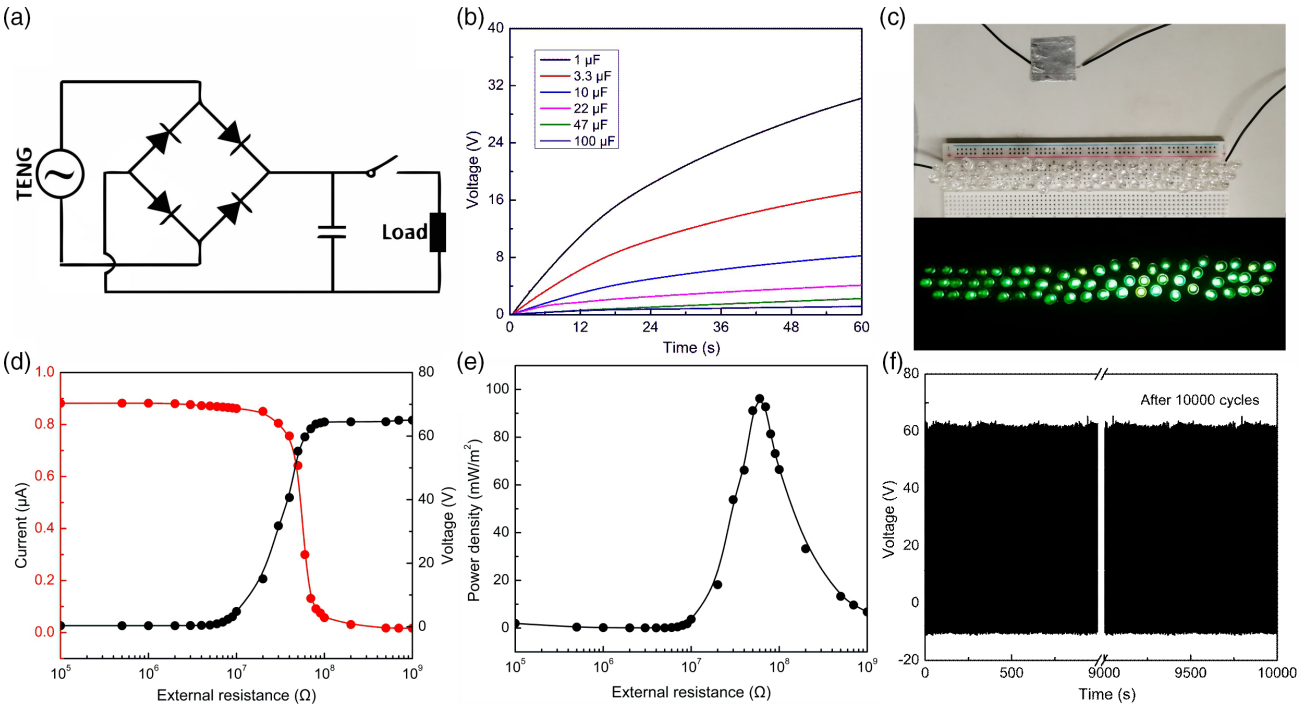

Figure 7. a) The working electrical circuit of the charging system based on TENG. b) Charging behavior of the PDMS-black Cu-CFP based TENG with various capacitors (50 N, 1 Hz). c) Demonstrations of lighting up LEDs using a TENG working in hand hammering. d) The influence of the variable external resistance on the output current and voltage of TENG. e) The relationship between output power density and load resistances. f) The test of stability and durability for 10 000 cycles with the TENG (50 N, 1 Hz).

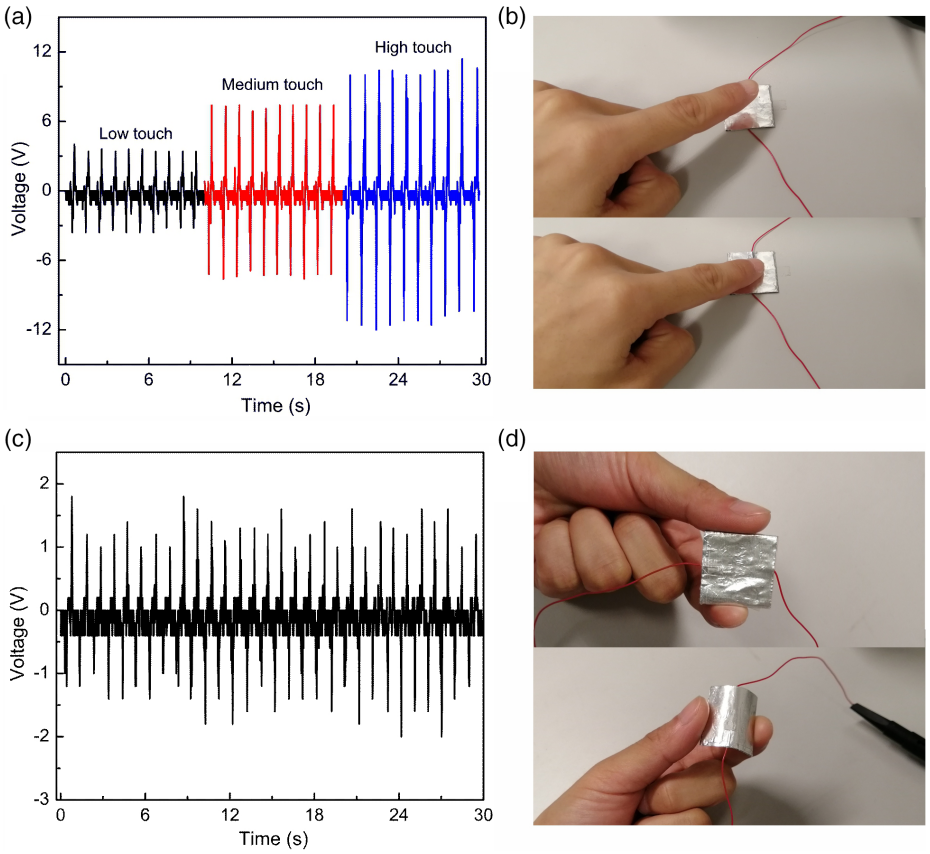

Figure 8. Demonstration of the TENG based tactile sensor. a) Output voltage b) photos generated by the TENG with varied finger touch. c) Output voltage d) photos generated under different bending conditions.

load is equal to the internal resistance of TENG. Therefore, when the load resistor is $6 \times 10^7\ \Omega$, the maximum output power density of 97.9 mW m^{-2} is achieved. Such a large amount of output power is sufficient to charge energy storage equipment, and drive certain flexible and wearable electronic devices, thereby expanding the application range of TENG.

Taking into consideration the important factor in real-life practical application, the long-term stability and durability of the equipment are also crucial factors that will influence its actual usage and lifetime. By evaluating the prepared TENG in 10 000 cycles of continuous operation (Figure 7f), the electrical output voltage of the PDMS-black Cu-CFP-based TENG can still remain stable without significant fluctuations, indicating that the prepared TENG has outstanding durability and stability. The mechanical stability of TENG at different bending angles in 1000 cycles was also evaluated. The output performance of the TENG decreases slightly at a small bending angle; when the bending angle is greater than 5 mm, it has almost no effect on the output performance (Figure S6, Supporting Information).

As the wearable TENG can obtain mechanical energy from human motion in daily life and convert it into electrical signals, the equipment was also used to observe different types of body movement, thereby realizing a self-charging biomechanical motion sensor system. The output voltage of sensor based on the TENG under kinds of human movements, such as bending and finger touching, was recorded. To further test the response of the TENG-based sensor to forces of different intensities from the human body, we applied three different forces (low ≈2 N, medium ≈4 N, and high touch ≈7 N, respectively) to touch the prepared TENG with our fingers (Movie S2, Supporting Information). **Figure 8**a,b shows three various curves, corresponding to peak voltage outputs of 3.6, 7.7, and 11.4 V, respectively, which proves that TENG is very sensitive to different touch force.

To prove its flexibility and the potential in monitoring human motion, the electrical output performance with various bending degrees was further studied. As shown in Figure 8c,d, the TENG device produces a distinctive output voltage curve with random bending degrees. The results show that the flexibility and sensitivity of the TENG device are sufficient to produce electrical output responses to various degrees of bending.

3. Conclusions

In summary, we fabricated black Cu-coated CFP by ELD technique in a new way to obtain high electrical output performance of TENG due to the reduction of the internal resistance of PDMS and the bulk thickness of the dielectric material. The synergistic effect of black Cu NPs and CFP embedded in the PDMS matrices significantly improves the charge transportation, while the

PDMS-black Cu-CFP-based TENG produces the highest surface charge density with a high sensitivity of 1.56 V N^{-1}, which is 3.5 times of that obtained via PDMS-based TENG under the same condition. Such a novel extension of ELD technology not only is an effective approach for preparing TENG with high electrical output performance and TENG-based tactile sensor with high sensitivities, but also provides a new perspective for inspiring excellent applications in the domains of wearable devices, artificial skin, catalysis, photothermal conversion, biomedical industries, and so on.

4. Experimental Section

Materials: All chemicals were purchased from Sigma-Aldrich.

Polymer Surface Modification: Tannic acid (TA) was dissolved in deionized water to prepare an aqueous solution of TA (5 g L^{-1}). After the CFP film was immersed in the solution for 15 min, the obtained TA-modified CFP was rinsed with deionized water several times for cleaning.

Electroless Deposition: The catalyst was immobilized by dipping the TA-treated CFP in a 5×10^{-3} M $(NH_4)_2PdCl_4$ aqueous solution for 15 min. By thoroughly washing the $PdCl_4^{2-}$ immobilized CFP film with deionized water, the excess physical absorption of the catalyst can be removed. The Cu plating solution was prepared in an ELD bath containing a mixture of freshly prepared solutions A, B, and deionized water at room temperature in a volume ratio of 1:1:2. Solution A consisted of 18 g L^{-1} NaOH, 43.5 g L^{-1} $KNaC_4H_4O_6{\cdot}4H_2O$, and 19.5 g L^{-1} $CuSO_4{\cdot}5H_2O$. Solution B was a freshly prepared reducing agent solution including 14.5 mL L^{-1} HCHO in deionized water. After Cu ELD process, the samples were cleaned with deionized water several times and dried in a vacuum oven.

Fabrication of Self-Powered Tactile Sensor: Finally, the obtained black Cu-coated CFP was immersed in the viscous PDMS precursor once (Sylgard 184, DowCorning, USA), which was prepared by mixing silicone elastomer and the curing agent at a mass ratio of 10:1 and then cured in an oven. After that, the prepared composite films were cut into a square with dimensions of 2.5 × 2.5 cm^2 for use as the dielectric layer in the TENG structure. One piece of Al foil was directly attached to one surface of the PDMS-black Cu-coated CFP film as the electrode, and another piece of Al foil replaced the skin as the positive friction material. At the same time, to simulate the actual working situation of the self-powered sensor is close contact with the human body during real work, only double-sided tape (thickness: 80 μm) was used as an insulator by fixing the four sides of PDMS-black Cu-coated CFP film to ensure that there was a gap between the simulated skin layer (Al foil) and the PDMS-black Cu-coated CFP film. Cu wires were connected to the electrode using a silver paste.

Characterization: Fourier transform infrared spectroscopy (PerkinElmer Paragon 100 FT-IR) performed in the attenuated total reflectance (ATR) mode was used to prove the modification of TA on CFP. The surface chemical composition of catalyst-immobilized CFP was analyzed by X-ray photoelectron spectroscopy (XPS, Thermo Scientific Nexsa, USA). The structure of black Cu particles on the CFP surface was characterized by X-ray diffractometer (XRD, Rigaku SmartLab 9 kW-Advance, Japan). The surface morphology of the samples was investigated by scanning electron microscopy (SEM, Tescan MAIA3, Czech), and energy-dispersive X-ray spectroscopy (EDS) was adopted at the same time for element analysis. The dielectric constant was measured using a precision LCR meter (Keysight E4980A).

The Keyboard Life Tester (ZX-A03) was used to test the output performance of the developed TENGs, which can supply a continuous dynamic up and down movement with a controlled frequency of 1–5 Hz. The applied force was checked by a force sensor (Model: ZNHB-P-5KG and ZN5S-FG, China). The output voltage was measured with the RIGOL DS1054Z oscilloscope. An electrometer (Keithley 6514) was used to measure the output current and the transferred charge.

Supporting Information

Supporting Information is available from the Wiley Online Library or from the author.

Acknowledgements

M.Y. would like to thank the Hong Kong Polytechnic University for providing her with a postgraduate scholarship.

Conflict of Interest

The authors declare no conflict of interest.

Data Availability Statement

The data that support the findings of this study are available from the corresponding author upon reasonable request.

Keywords

black Cu, cellulose filter paper, electroless deposition, polydimethylsiloxane, tactile sensing, triboelectric nanogenerators

Received: June 2, 2021
Revised: July 6, 2021
Published online: August 5, 2021

[1] H. R. Lim, H. S. Kim, R. Qazi, Y. T. Kwon, J. W. Jeong, W. H. Yeo, *Adv. Mater.* **2020**, *32*, 1901924.
[2] K. Dong, X. Peng, Z. L. Wang, *Adv. Mater.* **2019**, *32*, 1902549.
[3] F. R. Fan, W. Tang, Z. L. Wang, *Adv. Mater.* **2016**, *28*, 4283.
[4] H. Wu, Z. Su, M. Shi, L. Miao, Y. Song, H. Chen, M. Han, H. Zhang, *Adv. Funct. Mater.* **2017**, *28*, 1704641.
[5] X. He, Y. Zi, H. Yu, S. L. Zhang, J. Wang, W. Ding, H. Zou, W. Zhang, C. Lu, Z. L. Wang, *Nano Energy.* **2017**, *39*, 328.
[6] F. Wen, H. Wang, T. He, Q. Shi, Z. Sun, M. Zhu, Z. Zhang, Z. Cao, Y. Dai, T. Zhang, C. Lee, *Nano Energy.* **2020**, *67*, 104266.
[7] G. Ferreira, S. Goswami, S. Nandy, L. Pereira, R. Martins, E. Fortunato, *Adv. Funct. Mater.* **2020**, *30*, 1908994.
[8] D. H. Ho, J. Han, J. Huang, Y. Y. Choi, S. Cheon, J. Sun, Y. Lei, G. S. Park, Z. L. Wang, Q. Sun, J. H. Cho, *Nano Energy* **2020**, *77*, 105262.
[9] K. Dong, Z. Wu, J. Deng, A. C. Wang, H. Zou, C. Chen, D. Hu, B. Gu, B. Sun, Z. L. Wang, *Adv. Mater.* **2018**, *30*, 1804944.
[10] S. A. Graham, B. Dudem, A. R. Mule, H. Patnam, J. S. Yu, *Nano Energy.* **2019**, *61*, 505.
[11] J. Han, C. Xu, J. Zhang, N. Xu, Y. Xiong, X. Cao, Y. Liang, L. Zheng, J. Sun, J. Zhai, Q. Sun, Z. L. Wang, *ACS Nano* **2021**, *15*, 1597.
[12] L. Huang, S. Lin, Z. Xu, H. Zhou, J. Duan, B. Hu, J. Zhou, *Adv. Mater.* **2019**, *32*, 1902034.
[13] F. Yi, Z. Zhang, Z. Kang, Q. Liao, Y. Zhang, *Adv. Funct. Mater.* **2019**, *29*, 1808849.
[14] Z. Li, K. Hu, M. Yang, Y. Zou, J. Yang, M. Yu, H. Wang, X. Qu, P. Tan, C. Wang, X. Zhou, Z. Li, *Nano Energy.* **2019**, *58*, 852.
[15] H. Kang, C. Zhao, J. Huang, D. H. Ho, Y. T. Megra, J. W. Suk, J. Sun, Z. L. Wang, Q. Sun, J. H. Cho, *Adv. Funct. Mater.* **2019**, *29*, 1903580.
[16] Y. Jie, Q. Jiang, Y. Zhang, N. Wang, X. Cao, *Nano Energy.* **2016**, *27*, 554.

[17] J. Yu, X. Hou, J. He, M. Cui, C. Wang, W. Geng, J. Mu, B. Han, X. Chou, *Nano Energy.* **2020**, *69*, 104437.
[18] L. Lu, B. Yang, Y. Zhai, J. Liu, *Nano Energy.* **2020**, *76*, 104966.
[19] J. Xiong, P. Cui, X. Chen, J. Wang, K. Parida, M. Lin, P. Lee, *Nat Commun.* **2018**, *9*, 4280.
[20] S. Wang, L. Lin, Z. L. Wang, *Nano Energy.* **2015**, *11*, 436.
[21] Y. Yang, J. Han, J. Huang, J. Sun, Z. L. Wang, S. Seo, Q. Sun, *Adv. Funct. Mater.* **2020**, *30*, 1909652.
[22] J. Huang, X. Yang, J. Yu, J. Han, C. Jia, M. Ding, J. Sun, X. Cao, Q. Sun, Z. L. Wang, *Nano Energy.* **2020**, *69*, 104419.
[23] S. Li, J. Nie, Y. Shi, X. Tao, F. Wang, J. Tian, S. Lin, X. Chen, Z. L. Wang, *Adv. Mater.* **2020**, *32*, 2001307.
[24] B. Yu, H. Yu, H. Wang, Q. Zhang, M. Zhu, *Nano Energy.* **2017**, *34*, 69.
[25] K. Yao, Y. Liu, D. Li, J. He, J. Li, R. H. W. Lam, Z. Xie, L. Wang, X. Yu, *Nano Energy.* **2020**, *76*, 105017.
[26] L. Zhao, Q. Zheng, H. Ouyang, H. Li, L. Yan, B. Shi, Z. Li, *Nano Energy.* **2016**, *28*, 172.
[27] G. Li, G. Wang, Y. Cai, N. Sun, F. Li, H. Zhou, H. Zhao, X. Zhang, J. Han, Y. Yang, *Nano Energy.* **2020**, *75*, 104918.
[28] A. R. Mule, B. Dudem, S. A. Graham, J. S. Yu, *Adv. Funct. Mater.* **2019**, *29*, 1807779.
[29] Y. Mao, Y. Li, J. Xie, H. Liu, C. Guo, W. Hu, *Nano Energy* **2021**, *84*, 105918.
[30] K. Shi, X. Huang, B. Sun, Z. Wu, J. He, P. Jiang, *Nano Energy* **2019**, *57*, 450.
[31] J. Kim, W. Kim, G. Jang, D. S. Hyeon, M. H. Park, J. P. Hong, *Adv Energy Mater.* **2019**, *10*, 1D.
[32] J. Chen, H. Guo, X. He, G. Liu, Y. Xi, H. Shi, C. Hu, *ACS Appl. Mater. Interfaces* **2016**, *8*, 736.
[33] X. He, X. Mu, Q. Wen, Z. Wen, J. Yang, C. Hu, H. Shi, *Nano Res.* **2016**, *9*, 3714.
[34] X. Yang, W. A. Daoud, *Adv. Funct. Mater.* **2016**, *26*, 8194.
[35] Y. Yu, Z. Li, Y. Wang, S. Gong, X. Wang, *Adv. Mater.* **2015**, *27*, 4938.
[36] S. Sriphan, T. Charoonsuk, T. Maluangnont, P. Pakawanit, C. Rojviriya, N. Vittayakorn, *Adv Mater Technol.* **2020**, *5*, 2000001.
[37] J. Chun, J. W. Kim, W. Jung, C. Kang, S. Kim, Z. L. Wang, J. M. Baik, *Energ Environ Sci.* **2015**, *8*, 3006.
[38] M. Pusty, P. M. Shirage, *Rsc Adv.* **2020**, *10*, 10097.
[39] W. He, M. Sohn, R. Ma, D. J. Kang, *Nano Energy.* **2020**, *78*, 105383.
[40] C. Jiang, X. Li, Y. Yao, L. Lan, Y. Shao, F. Zhao, Y. Ying, J. Ping, *Nano Energy* **2019**, *66*, 104121.
[41] X. Yang, W. A. Daoud, *J. Mater Chem A* **2017**, *5*, 9113.
[42] M. Kim, M. Kim, H. Kwon, S. Jo, Y. Kim, *RSC Adv.* **2017**, *7*, 48368.
[43] X. Xia, J. Chen, G. Liu, M. S. Javed, X. Wang, C. Hu, *Carbon* **2017**, *111*, 569.
[44] L. Wang, X. Yang, W. A. Daoud, *Nano Energy.* **2019**, *55*, 433.
[45] B. D. Chen, W. Tang, C. Zhang, L. Xu, L. P. Zhu, L. J. Yang, C. He, J. Chen, L. Liu, T. Zhou, Z. L. Wang, *Nano Res.* **2018**, *11*, 3096.
[46] K. Shi, H. Zou, B. Sun, P. Jiang, J. He, X. Huang, *Adv. Funct. Mater.* **2020**, *30*, 1904536.
[47] P. Li, Y. Zhang, Z. Zheng, *Adv. Mater.* **2019**, *31*, 1902987.
[48] C. Zhu, E. Chalmers, L. Chen, Y. Wang, B. B. Xu, Y. Li, X. Liu, *Small.* **2019**, *15*, 1902440.
[49] T. Søndergaard, S. M. Novikov, T. Holmgaard, R. L. Eriksen, J. Beermann, Z. Han, K. Pedersen, S. I. Bozhevolnyi, *Nat. Commun.* **2012**, *3*, 969.
[50] Z. L. Wang, A. C. Wang, *Mater Today* **2019**, *30*, 34.
[51] S. Chen, J. Jiang, F. Xu, S. Gong, *Nano Energy* **2019**, *61*, 69.